JOURNAL OF GEOPHYSICAL RESEARCH, VOL. 104, NO. C6, PAGES 13,431–13,448, JUNE 15, 1999

Modeling the seasonal variability of hydrography and circulation in the Kara Sea

I. H. Harms

Institute for Marine Research, University of Hamburg, Hamburg, Germany

M. J. Karcher[1]

Federal Maritime and Hydrographic Agency, Hamburg, Germany

Abstract. In the frame of a project on transport of contaminants in the Arctic, the Hamburg shelf ocean model (HAMSOM) is applied to the Kara Sea. The HAMSOM system consists of a three-dimensional, baroclinic circulation model coupled to a thermodynamic and dynamic sea ice model. The Kara Sea model is forced with climatological winds, atmospheric heat fluxes, river runoff, and tides. The obtained results reveal no typical Kara Sea circulation that prevails throughout the year. Instead, the model showed a strong seasonal variability in circulation and hydrography due to winds, freshwater runoff, and ice formation. The circulation is weakest in spring when the wind speeds are low and horizontal density gradients are small. Fresh water from the rivers spreads toward the north and northwest rather than forming a coastally trapped current that flows to the east. In autumn, the circulation is significantly enhanced because of increasing wind speeds and strong horizontal density gradients. Good agreement was found between model results and recent observations. The "classical" cyclonic current pattern in the southern Kara Sea, however, was not reproduced by the model.

1. Motivation

Over the past 5 years, several publications reported on increasing environmental problems in the Arctic Ocean and the Kara Sea (overview is given by *Nilsson* [1997]). One prominent example of Arctic pollution is the dumping of radioactive waste by the former Soviet Union [*Yablokov et al.,* 1993] which provided the motivation for intense experimental fieldwork [*Joint Russian-Norwegian Expert Group,* 1996] and model studies on radionuclide transport in Arctic Shelf seas [*Scott et al.,* 1997; *Harms,* 1997b]. The great Siberian rivers that drain huge land areas and industrial zones may also contribute to the input of pollutants into the Arctic environment. In addition, intense oil and gas exploitation which is planned for the Kara Sea and finally the operation of the Northern Sea Route may cause environmental problems [*Moe et al.,* 1997].

In 1994, a joint project was initiated by the German Federal Maritime and Hydrographic Agency and the University of Hamburg (Institute for Marine Research) to investigate transport and dispersion of contaminants in the Arctic Ocean. The major goal of this work was to improve the oceanographic knowledge of the Arctic and the Kara Sea with respect to pathways and transit times of possible contaminants. Several numerical models were used in this project to evaluate present and future environmental problems of that region.

The present model study is part of this project and investigates circulation and hydrography of the Kara Sea with special emphasis on the seasonal variability. Section 2 describes the model used and section 3 presents the results. A summary and discussion are given in section 4.

2. Kara Sea Model

The Kara Sea model is based on the coding of the Hamburg shelf ocean model (HAMSOM) which is briefly described in section 2.1 and 2.2. A more detailed description of HAMSOM with applications to coastal waters and Arctic Shelf seas is given by *Stronach et al.* [1993], *Harms* [1994], and *Harms* [1997a]. Special emphasis is given to the application of the forcing data which is described in section 2.3.

2.1. HAMSOM system

HAMSOM is a three-dimensional, baroclinic circulation model, developed at the Institute of Marine Research (University Hamburg) for investigations of shelf sea processes [*Backhaus,* 1985]. The level-type model is based on nonlinear primitive equations of motion, invoking the hydrostatic approximation and the equation of continuity which serves to predict the elevation of the free surface from the divergence of the depth mean transport. The numerical scheme of the circulation model is semi-implicit, and the equations are discretized as finite differences on an Arakawa C-grid.

Vertical sub-grid scale turbulence is parameterized by means of a turbulent closure approach, proposed by *Kochergin* [1987] and later modified by *Pohlmann* [1996]. The scheme is closely related to a *Mellor and Yamada* [1974] level-2 model where vertical eddy viscosity coefficients depend on stratification and vertical current shear. Convective overturning is parameterized by vertical mixing: an unstable stratification is turned into a neutral state through artificial enlargement of the vertical eddy

[1]Now at Alfred-Wegener-Institute for Polar and Marine Research, Bremerhaven, Germany

Paper number 1999JC900048.
0148-0227/99/1999JC900048$09.00

viscosity coefficient. The horizontal diffusion of momentum is calculated using a constant, isotropic eddy viscosity coefficient.

The circulation model includes an Eulerian transport algorithm for temperature, salinity, and passive tracers based on the advection-diffusion equation and an upstream scheme. Vertical eddy diffusivity coefficients are calculated in the same way as vertical eddy viscosity coefficients, depending on stratification and vertical current shear. Horizontal eddy diffusion is neglected because of numerical diffusion stemming from the advection scheme. This artificial horizontal diffusion is related to the advection velocity, the average grid size, and the time step. For small and moderate velocities (< 0.3 m/s), which are typical for the simulated Kara Sea circulation, the artificial diffusion remains below 10^3 m^2/s.

The circulation model is coupled to a thermodynamic and dynamic sea ice model which calculates space and time dependent variations of ice thickness and ice concentration. The basic configuration follows *Hibler's* [1979] one-layer sea ice model. The classification constant for thin and thick ice is set in our case to 0.2 m. Ice thinner than this value is treated thermodynamically as open water. Thermodynamic changes in ice thickness and concentration depend principally on the sum of the involved heat fluxes. Latent and sensible heat fluxes at the ocean- or ice-atmosphere interfaces are calculated with standard bulk formulae [*Maykut,* 1986] on the basis of air temperatures, humidity, and cloud cover. Additional heat fluxes encompass the conductive heat flux through the ice, the turbulent heat flux under the ice, the long-wave radiation, and the incoming short-wave radiation. Salt fluxes due to brine release and ice melting are proportional to thermodynamic ice growth [*Lemke et al.* 1990]. A constant and isotropic ice salinity of 10 practical saliniy units (psu) is used which is related mainly to thin ice and new ice formation.

The dynamic part of the ice model is kept simple and does not include an ice rheology. Instead, a "free drift" algorithm accounts for advection of ice thickness and ice concentration due to wind and water stress at the surface or the bottom of the ice [*Bruno and Madsen,* 1989]. This approach was chosen in order to reduce the computer time for tracer simulations over long time spans. The calculation of the wind stress at the ice or water surface follows a second-order approach with individual wind drag coefficients for water and ice [*McPhee,* 1979]. In order to account for landfast ice, the ice drift in winter should be suppressed in very shallow regions with depth < 20 m. However, a "numerical switch" between normal ice movement (depth > 20 m) and no ice movement (depth < 20 m) caused rather unrealistic discontinuities not only in the ice velocities but also in ice thickness and concentration. In order to smooth this effect, we decided to define a "transition zone" between regions with more than 50 m depth, where the ice drift is free and regions with less than 20 m depth, where the ice drift is set to zero. This interpolation algorithm is applied only in winter (i.e. January, February, and March). It will be shown in section 3.1.1. that this rather simple dynamic approach reproduces observed ice thickness and concentrations in the Kara Sea remarkably well.

2.2. Model Configuration

The HAMSOM-system is applied with high spatial resolution to the central Kara Sea (Figure 1). The domain includes very shallow areas (< 50 m) along the Siberian coast, the river estuaries of Ob and Yenisei as well as the deep Novaya Semlya Trough (> 400 m). The topography is based mainly on the ETOPO 5 data set [*Hirtzler,* 1985]. Some smaller corrections were made according to sea charts of that region [*Perry and Fleming,* 1986; *Cherkis et al.,* 1990] and topographic data sets from other model applications [*Kowalik and Proshutinsky,* 1993]. The Kara Strait (to the Barents Sea) and the Vilkitsky Strait (to the Laptev Sea) represent open boundaries to the model. The northern parts of the Kara Sea, namely, the Svyataya Anna Trough, were excluded since these areas are strongly influenced by the Barents Sea outflow toward the Arctic. The grid of the model is equidistant with a mesh size of 9.4 km. The vertical scale is resolved with 12 layers having boundaries in 5, 10, 15, 25, 50, 75, 100, 150, 200, 300, 400, and 500 m depths.

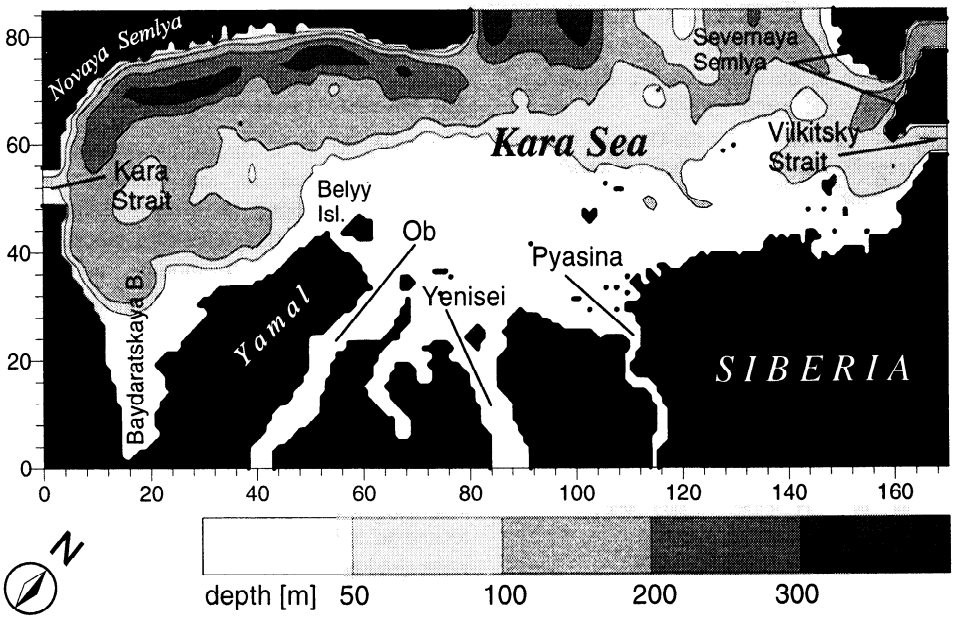

Figure 1. Domain and topography of the Kara Sea model.

The size of the matrix is 85 by 170, resulting in 50,051 wet grid points.

If not mentioned otherwise, a zero-gradient condition is applied at all open boundaries to (1) the horizontal velocity components for ice and water movement, to (2) temperature and salinity, and also to (3) ice concentration and ice thickness. The sea surface elevation at open boundaries is prescribed. The calculation of boundary values encompasses the inverse barometric effect coming from the air pressure, the geostrophic adjustment of the baroclinic field, and the tides (see section 2.3).

2.3. Applied Forcing Data

The application of numerical models to Arctic Shelf seas is very different from applications to well-known areas such as the North Sea or the Baltic Sea. The quality and quantity of forcing data is usually critical in Arctic Shelf regions, and a validation of model results is a difficult task. The intention of the paper is therefore also to describe the forcing data in order to evaluate their role in affecting the seasonal variability of circulation and hydrography. The Kara Sea model is forced with (1) M_2-tides, (2) monthly mean climatological data for wind speed and direction, (3) monthly mean climatological data for air temperature, cloud cover, and humidity, (4) 10-day mean river runoff data, (5) 10-day mean Kara Strait throughflow data, and (6) initial temperature and salinity fields.

The following five paragraphs describe the main characteristics of the applied forcing in more detail. Section 2.3.1. summarizes briefly the results from tidal simulations which were achieved using a previous barotropic/no-ice version of the Kara Sea model.

2.3.1. Tides. The Kara Sea Model accounts for the dominant M_2 tidal constituent. Amplitudes and phases were taken from a tidal model of the Arctic Ocean [*Kowalik and Proshutinsky*, 1994] and applied to the open boundaries. A comparison with observations and other model results [*Kowalik and Proshutinsky*, 1994; *Gjevik and Straume*, 1989] showed that the agreement is very good in the deeper central and southwestern parts of the Kara Sea, where the tidal influence is strong (see below). In very shallow northeastern parts, however, the comparison revealed some smaller differences (20 - 30%) between computed and observed amplitudes or phases (Table 1). In two cases, the differences were higher than 40%. This can be attributed to the northeastern open boundary of the model which unfortunately cuts through an amphidromic point west of Severnaya Semlya. The tidal solution proved to be sensitive to prescribed amplitudes and phases there. Another reason for differences might be the model topography which may reproduce the very shallow, complex bottom relief insufficiently.

Simulated M_2 tidal elevations are dominated by an amphidromic point in the western Kara Sea which is forced by a 180° phase lag of the incoming tidal wave between the Kara Strait and the open boundary to the Arctic Ocean. Simulated amplitudes (Figure 2a) usually remain below 20 cm except in two areas: the southern "Baydaratskaya" Bay area, where tidal resonance causes amplitudes of more than 70 cm, and the area north of Yamal peninsula around Belyy Island (30 - 35 cm).

Simulated maximum tidal currents (Figure 2b) are strongest in the Baydaratskaya Bay and near the river estuary of the Ob (30 cm/s). In the small strait between Yamal and Belyy Island, tidal currents may exceed 50 cm/s due to considerable horizontal gradients in tidal elevation. Preliminary tracer simulations [*Karcher et al.*, 1997] showed that these areas are significantly influenced by tidal mixing. Other regions, in particular those to the east of Novaya Semlya and in the eastern Kara Sea (along the Siberian coast) are only weakly influenced by the M_2 tides.

Residual currents can usually be found in shallow areas where tidal currents are strong. Again, this holds true for the Ob estuary, the area north of Yamal peninsula (around Belyy Island), and the Baydaratskaya Bay. However, the velocities are generally small and remain below 2 cm/s. Around Belyy Island, residual currents form a weak anticyclonic circulation.

Table 1. Comparison Between Observed and Simulated Amplitudes and Phases of the M_2 tide in the Kara Sea.

		Observed		Simulated	
Station	Name	Amplitude cm	Phase deg	Amplitude cm	Phase deg
186	Yugorskiy Shar	22	351	26	355
188	Ytsi Kara	21	48	29	50
189	Maaresaale	11	18	9	20
190	Harasavey	17	24	26	30
191	Belyi	23	129	23	150
197	Zjelania	16	150	16	165
199	Uedinenia Island	10	195	6	195
200	Izvestiy Ctik Island	11	195	7	210
201	Isachenko Island	8	180	7	205
202	Pravdy Island	18	201	15	235
204	Taymir Island	19	159	19	240
205	Russkyi Island	16	159	14	240
208	Krasnoflotskie Island	17	159	13	275
222	Dikson	10	318	7	320
223	Leskin Island	17	345	17	345
224	Obskaya Guba	32	357	16	360

The station numbers refer to locations in Figure 2.

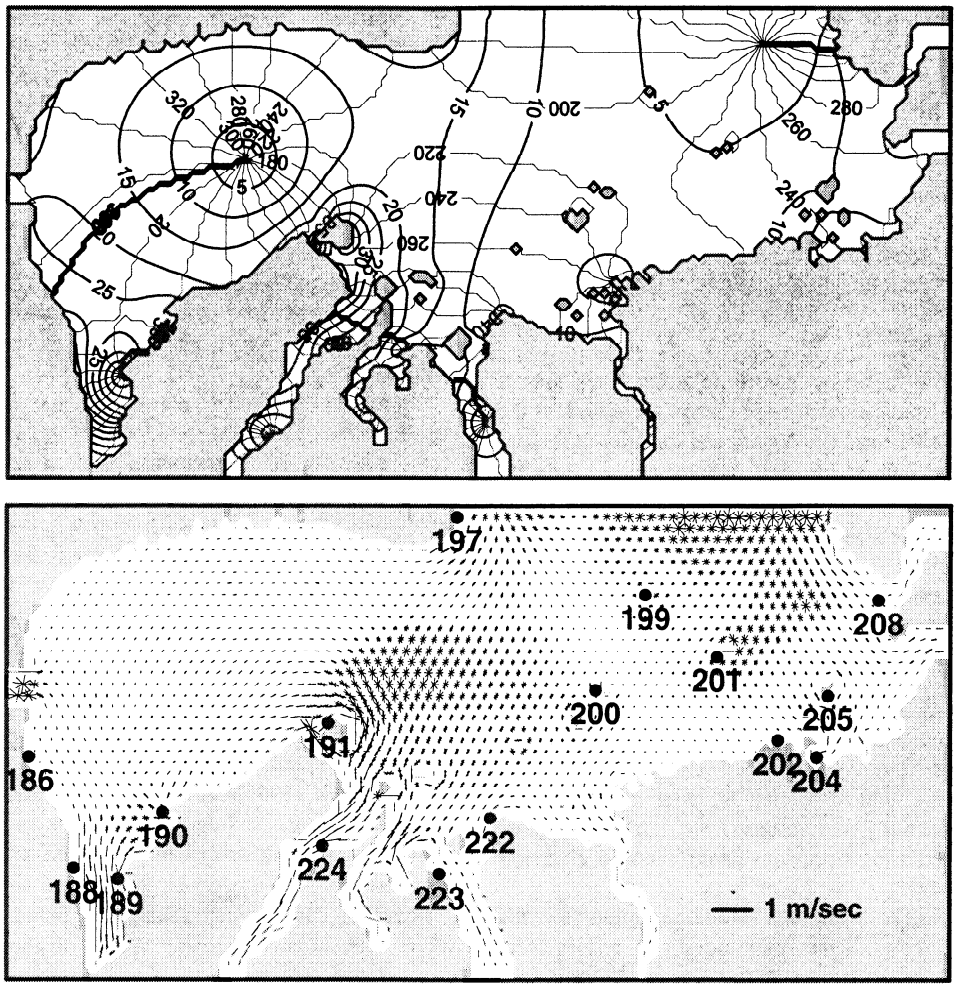

Figure 2. (a) Simulated amplitudes (5-cm intervals) and phases (20° intervals) of the M_2 tide in the Kara Sea. (b) Simulated M_2 tidal currents over one tidal cycle (tidal ellipses). Station numbers refer to locations described in Table 1.

2.3.2. Atmospheric forcing. The Kara Sea model is forced with monthly mean climatological wind stress values, deduced by *Trenberth et al.* [1989] from European Centre for Medium-Range Weather Forcast data [1988] for the period 1980-1989. The obtained wind fields (Figure 3) show strong, monsoon-like variability due to the seasonal air pressure distribution over the Arctic.

In winter, the Kara Sea is in a transition zone between a large and stable high- pressure cell over central Siberia and low-pressure ridges over the Barents and Norwegian Seas. Monthly mean wind speeds are high and very stable then, with maximum velocities of 8.5 m/s in February. From October to March, a cyclonic curl prevails with main wind directions from south to southwest for the central Kara Sea.

In summer, the air pressure distribution is reversed. The Siberian high-pressure cell decreases, and a high-pressure cell develops over the central Arctic. Horizontal air pressure gradients are much weaker, and the wind speeds are lower (2-4 m/s). The wind directions are more changeable, but north or northeast winds dominate.

Monthly mean climatological air temperature, humidity and cloud cover data were deduced by *Aukrust and Oberhuber* [1995] from ECMWF data for the period 1985-1990. The seasonal air temperature variance over Kara Sea waters is considerable and ranges from +5°C over the southwestern parts in August to -33°C over eastern parts in January. Compared to these strong variances, the relative humidity and the cloud cover remain quite stable during the whole year. The humidity is usually > 80%, and the cloud cover is between 60% and 80% in summer and > 80% in winter.

2.3.3. River runoff. The Kara Sea is dominated by large freshwater runoff in spring [*Pavlov et al.*, 1993]. The freshwater supply to the Kara Sea is mainly through the Ob and Yenisei rivers which drain a catchment area in Siberia and Russia of more than 5 million km^2. The total annual amount of freshwater input into the Kara Sea equals roughly 1200 km^3/yr, of which 80% is discharged in spring (May - June) [*Pavlov and Pfirman*, 1995].

Information on the river runoff to the Kara Sea was taken from an unpublished data review on the hydrology of Arctic rivers (O.F. Vasiliev et al., "Estimate of river water inflow to the Karsk Sea", Institute for Water and Environmental Problems, Siberian Branch, Russian Academy of Sciences, Novosibirsk, 1995). This review includes data of observed freshwater runoff rates from Siberian rivers for certain years. Apart from strong seasonal variations, the runoff values also showed interannual variations between "wet" and "dry" years. Tables 2 and 3 give yearly mean runoff rates in m^3/s for dry, wet and average years

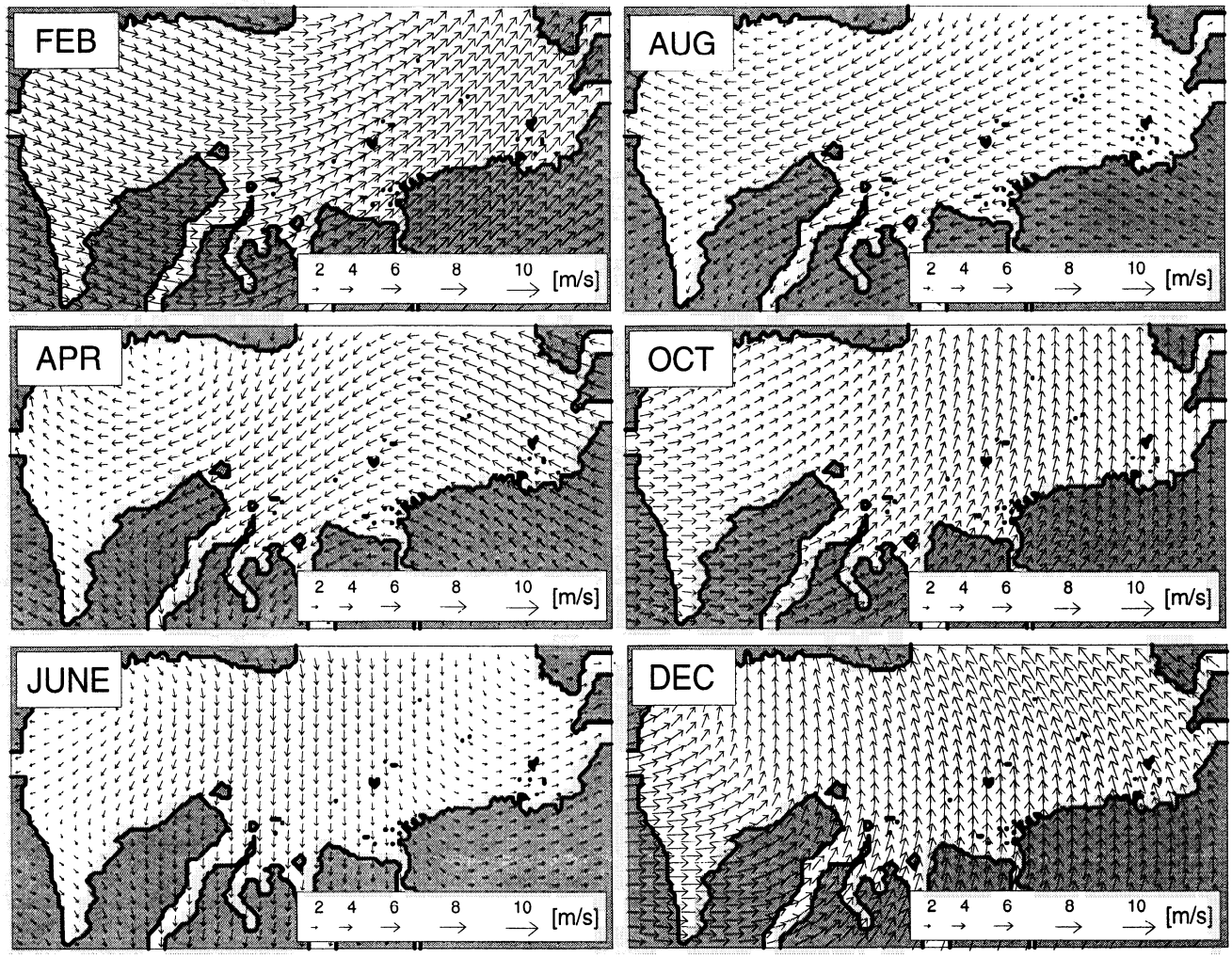

Figure 3. Applied climatological monthly mean wind direction and speed.

for the Ob and Yenisei rivers, respectively. In order to be consistent with the climatological atmospheric forcing, it was decided to use a realistic year with an average runoff for both rivers. This was found to be 1980, when the Ob and Yenisei rivers had yearly mean freshwater discharges of 12,700 m^3/s and 17,300 m^3/s, respectively.

In the Kara Sea model, the river runoff rates from the Ob, Yenisei and Pyasina are prescribed as 10-day mean volume fluxes in m^3/s (Figure 4). The Ob tributaries, Taz and Pur, are included in the Ob runoff. The salinity of the rivers at the point where they enter the model domain was set to 5 psu, whereas the temperature was prescribed depending on the season. Highest river temperature in August was set to 3.8°C; the lowest was during winter at the freezing point (-0.3°C).

Table 2. Selected yearly mean discharge rates of the Ob river.

Year	Conditions	Discharge rate
1987	most dry	8,490
1980	average	12,700
1979	most wet	18,200

Values are given in m^3/s. Source is an unpublished report "Estimate of river water inflow to the Karsk Sea", by O.F. Vasiliev et al., Institute for Water and Environmental Problems, Siberian Branch, Russian Academy of Sciences, Novosibirsk, 1995.

2.3.4. Kara Strait throughflow. The Barents Sea inflow through the Kara Strait is of major importance because it brings heat and salt into the Kara Sea. To account for these effects, the net inflow or outflow is prescribed as 10-day mean volume fluxes (Figure 5). These data were deduced from a coupled ice-ocean isopycnic general circulation model for the Arctic and sub-Arctic domains [*Karcher and Oberhuber,* 1997]. Temperature and salinity in the Kara Strait were prescribed according to the *Gorshkov* [1980] data atlas.

The simulated time series in Figure 5 suggests that the variability of the flow through the Kara Strait is mainly wind driven. Inflow from the Barents Sea is most enhanced during winter, when strong south to southwesterly winds prevail. The

Table 3. Selected yearly mean discharge rates of the Yenisei river.

Year	Conditions	Discharge rate
1968	most dry	15,500
1980	average	17,300
1995	most wet	20,900

Values are given in m^3/s. Source is an unpublished report "Estimate of river water inflow to the Karsk Sea", by O.F. Vasiliev et al., Institute for Water and Environmental Problems, Siberian Branch, Russian Academy of Sciences, Novosibirsk, 1995.

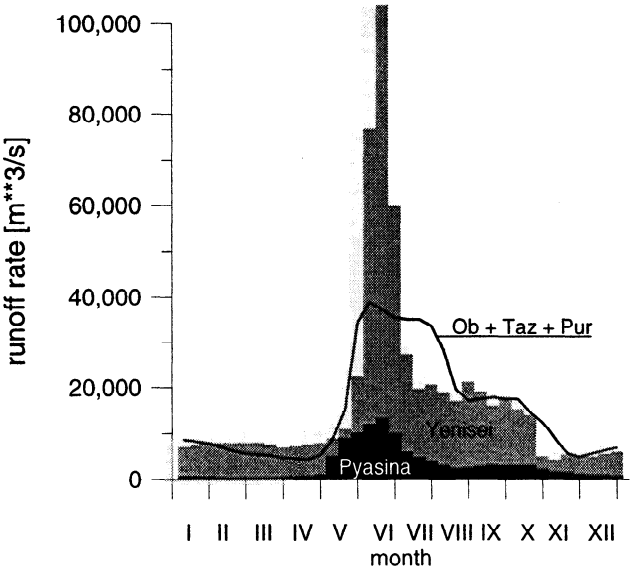

Figure 4. Applied 10-day mean river runoff from Ob (including tributaries Taz and Pur), Yenisei, and Pyasina rivers.

maximum transport rate into the Kara Sea is 0.65 Sv during the first half of January. In summer, when northerly winds prevail, the inflow is reduced, showing a slight net outflow (-0.07 Sv) toward the Barents Sea in July and August. The mean inflow averaged over 1 year is 0.3 Sv.

The computed time series of volume flux through the Kara Strait is in good agreement with observations of *Pavlov and Pfirman* [1995]. They estimated the yearly averaged inflow toward the Kara Sea to be in the range of 0.04 Sv up to 0.6 Sv. However, the seasonal variability of the throughflow is almost unknown, except for some single observations: "Historic" circulation patterns, deduced from hydrographic observations and direct current measurements, suggest a water exchange through the strait in both directions [*Pfirman et al.*, 1997]. According to these surface flow charts, the northern part of the strait is dominated by an outflow from the Kara Sea (the "Litke Current") whereas the southern part is dominated by an inflow from the Barents Sea. This bidirectional flow, which also appears in laboratory simulations (*T.A. McClimans*, personal communication, 1997), has been recently supported by satellite images from the Kara Strait, but only for the summer season. Advanced very high resolution radiometer (AVHRR) data from August 1988 and 1994 reveal considerable horizontal temperature gradients across the strait which might be due to horizontal current shear [*Pfirman et al.*, 1997]. Since there is no information on the winter situation, it remains unclear if this is a permanent or a seasonal feature.

The observed bidirectional flow in the Kara Strait is thought to be forced by northerly winds driving surface waters to the west and by the Pechora runoff which results in a density-driven coastal current, flowing to the east. Both features do not appear in winter; the runoff is absent and the winds are from south to southwest. It is therefore unlikely that the observed bidirectional flow is also present during winter. Looking at the wind direction and speed over the Kara Strait, it is more reasonable to assume that the Barents Sea inflow is much stronger from October to March than during the remaining part of the year. The computed time series of volume fluxes in Figure 5 supports these assumptions.

2.3.5. Temperature and salinity data. Because of severe climate conditions but also because of political reasons, the Kara Sea was relatively inaccessible during the last decades. This still seems to be the case, and results in a general lack of data for validation and forcing of numerical models. With respect to the high resolution of the applied model grid and in order to avoid the application of insufficiently resolved temperature and salinity data sets, the model is not constrained to any climatological data. Instead, it was decided to use reasonable initial fields for the start and to run the model in a full prognostic mode. Several test runs showed that the small grid size allows for a very detailed space resolution of, for example, frontal structures in the vicinity of the river plume which are found to be poorly resolved in available climatological data sets.

The model is started at rest in late winter, April 1. There is no ice at the sea surface. The initial temperature is set to the freezing point in the whole model domain following the description of *Pavlov et al.* [1993]. The initial salinity distribution is prescribed according to the spring data of *Levitus* [1982]. Applying these start conditions, the model needs a spin-up of at least one summer and one winter season to achieve reasonable results for circulation and hydrography.

3. Results

The Kara Sea model was run with the complete set of forcing functions in a prognostic mode for several years. After 3 years, the model reached an almost cyclic stationary state. This holds true, in particular, for the circulation, the sea surface elevations, and the temperatures which behave quite robustly. A more sensitive variable is the surface salinity. Simulations for time spans longer than 3 years revealed a small drift for the average surface salinity which is due to an imbalance between freshwater runoff, ice formation, and ice export.

The following model results are taken from the third year of simulation. We first describe the results concerning the

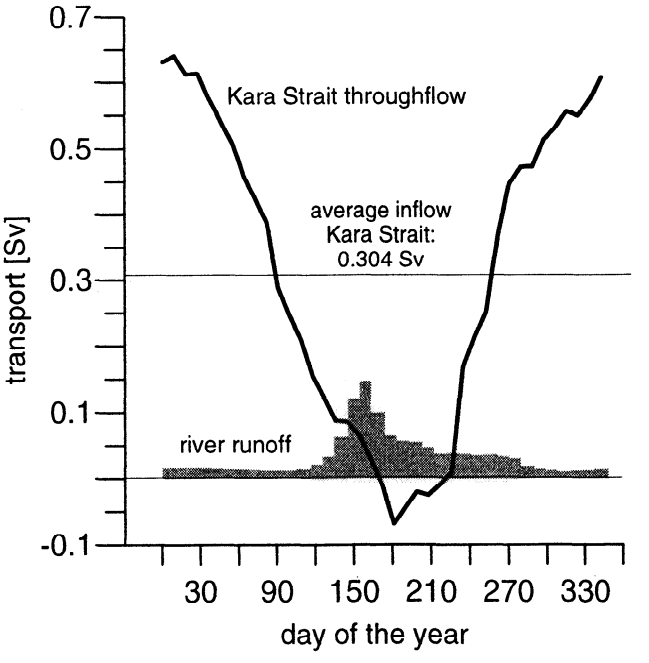

Figure 5. Prescribed Kara Strait throughflow, deduced from an Arctic isopycnic general circulation model [*Karcher and Oberhuber*, 1997]. The total river runoff is shown for comparison.

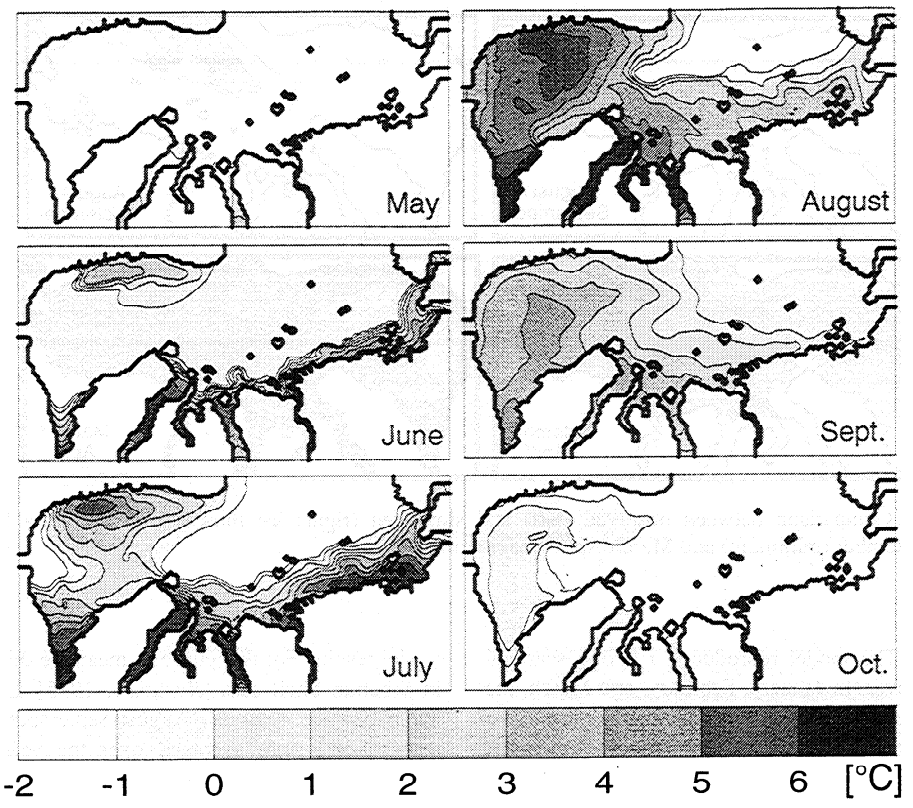

Figure 6. Simulated sea surface temperatures from May to October.

hydrography (section 3.1) followed by the circulation results in section 3.2. Where possible, the results are compared to observations or oceanographic descriptions such as the comprehensive summary on the Barents and Kara Seas given by *Pavlov et al.* [1993].

3.1. Hydrography

The following Section describes the simulated seasonal variability of the hydrography, focusing on sea surface temperatures (3.1.1), sea ice (3.1.2), sea surface salinity (3.1.3), and vertical stratification (3.2.4).

3.1.1. Sea surface temperature (SST). Because of a closed ice cover, the SST in the Kara Sea (Figure 6) is at the freezing point until April. In spring, the incoming short wave radiation is mainly used for ice melting which starts in May in the river estuaries and along the Siberian coast. In these ice-free areas, the inflowing river water mixes with melt water creating, together with atmospheric warming, a thin but very pronounced, warm and low saline surface layer. The spring ice melting is also strong along the east coast of Novaya Semlya where prevailing northerly winds drive the ice cover offshore. This allows the short wave radiation to penetrate into surface waters and to heat them. In July, August, and September, the southern Kara Sea is ice free. The highest surface temperatures occur in August near the Kara Strait and in the Baydaratskaya Bay (6°- 7°C). These values agree well with observed average summer temperatures in the southern Kara Sea given by *Pavlov et al.* [1993] and *Burenkov and Vasil'kov* [1995]. Because of a small remaining ice shield between Novaya Semlya and Severnaya Semlya, the SST does not rise significantly above the freezing points there.

Freezing starts already in September in the eastern parts and the surface temperatures drop rapidly during October and November in the whole Kara Sea. In the eastern parts of the Kara Sea, the ice cover establishes quite fast because of a pronounced haline stratification (river and melt water) which inhibits vertical mixing and heat transfer from below. In the western parts, however, where the Barents Sea inflow is dominating, the haline stratification is much weaker. Here vertical mixing and upward heat transfer are more intense, which hampers a rapid closing of the ice cover and keeps the autumn SST significantly higher than in the eastern parts. Until December, an almost closed ice cover is established also in the southern parts, and the SST is at (or close to) the freezing point.

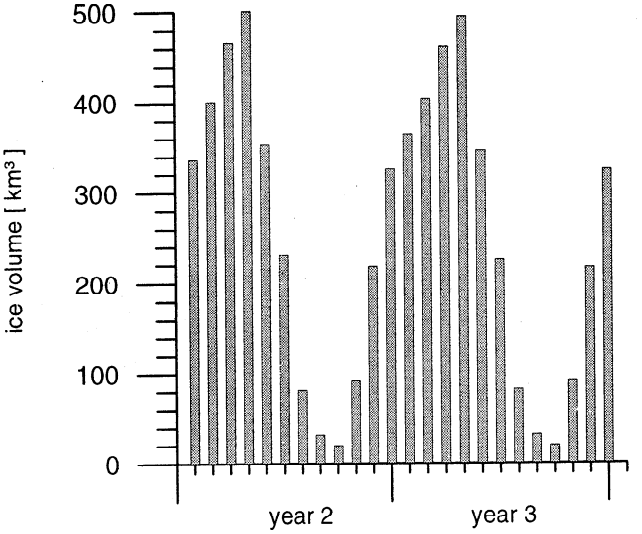

Figure 7. Simulated seasonal cycle of the ice volume in the Kara Sea model domain.

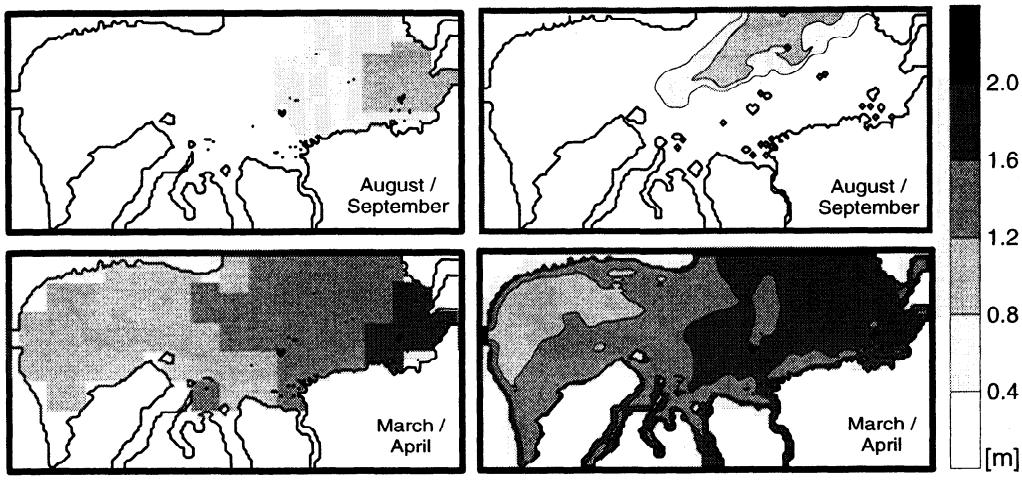

Figure 8. Comparison between observed (left) and simulated (right) ice thickness in the Kara Sea, during August/September (minimum) and March/April (maximum).

3.1.2. Sea ice. The model reproduces a strong seasonal variance of the ice cover. In January, February, and March, the Kara Sea is completely covered by ice with a maximum (average) ice thickness of 1.7 m. In August-September, however, the Kara Sea is almost totally ice free. Only a small ice shield remains between Novaya Semlya and Severnaya Semlya with an average ice thickness of 0.5 m. The seasonal variance of ice volume in the model domain is depicted in Figure 7; the ice volume decreases from almost 500 km^3 in April down to less than 50 km^3 in September.

Simulated ice thickness and concentrations are compared to climatological data (Figures 8 and 9) in order to evaluate the model results. For this purpose, mean ice thickness distributions in Siberian Shelf seas [*Romanov,* 1995] during minimum and maximum ice seasons (August-September and March-April, respectively) were averaged over the years 1972-1981. The comparison with model results (Figure 8) reveals a slight overestimation of the simulated ice thickness in winter, whereas the simulated summer ice thickness is somewhat underestimated along the Siberian coast. Instead, the model shows larger summer ice thickness between Novaya Semlya and Severnaya Semlya. It has to be mentioned, however, that the interannual variance of the original data (1972-1981) is considerable.

Mean ice concentrations for similar (minimum and

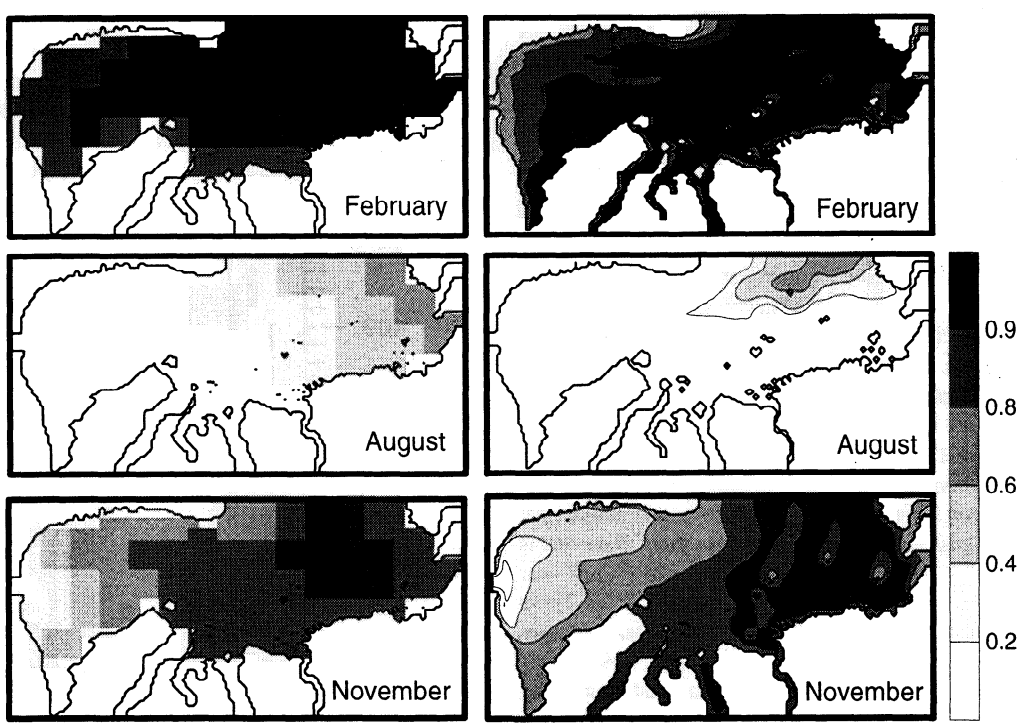

Figure 9. Comparison between observed (left) and simulated (right) ice concentrations in the Kara Sea during February, August, and November.

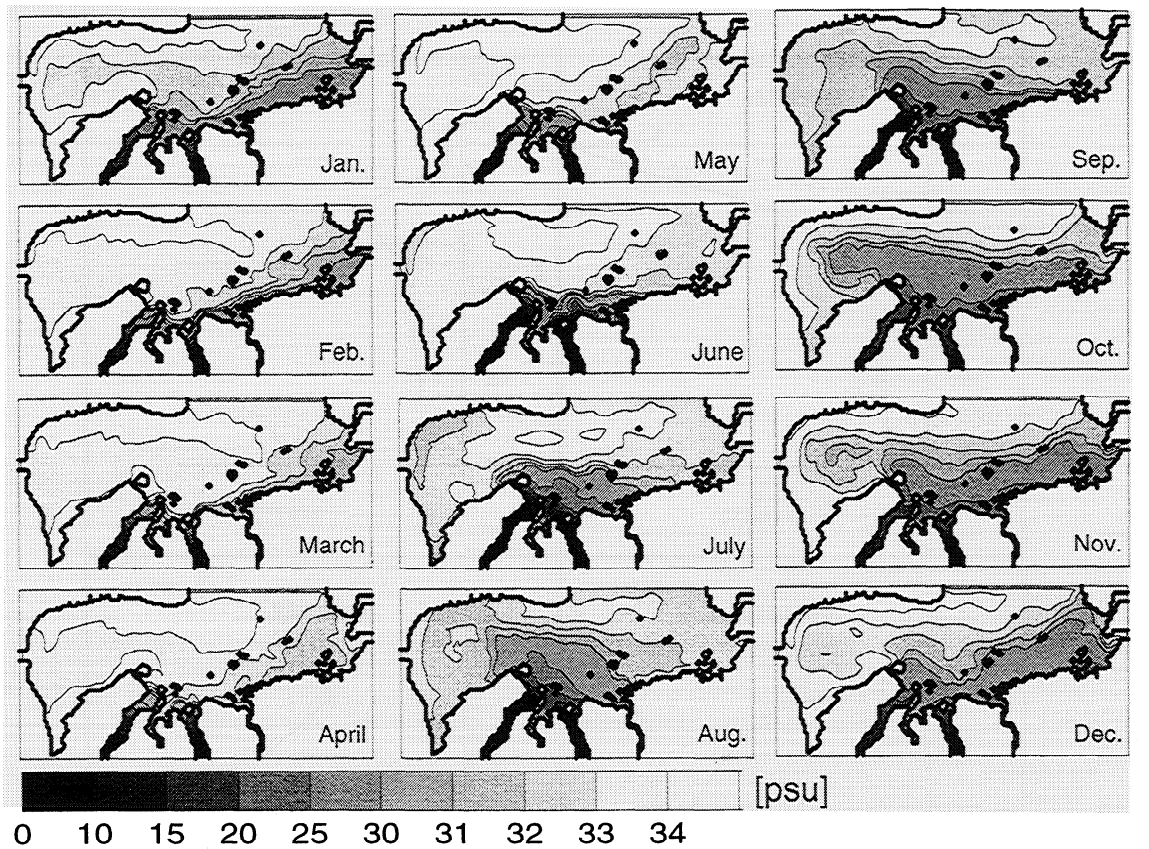

Figure 10. Simulated monthly mean sea surface salinity.

maximum) seasons are taken from satellite passive-microwave observations during the years 1978-1987 [*Gloersen et al.*, 1992]. We additionally compare the ice concentrations in November which is the main freezing month (Figure 9). Bearing in mind the rather simple "free drift" ice dynamics of the model, the comparison shows a remarkably good agreement. As with the ice thickness, a small disagreement can be seen in summer, when the simulated ice concentration in the northeastern parts is underestimated.

The rather good agreement between winter observations and simulations can be attributed to the fact that the Kara Sea is an ice export region, where thermodynamic ice formation and divergent (offshore) ice movement dominates. A prevailing convergent ice movement (onshore), which can be assumed in summer in the eastern parts, leads to specific dynamic processes such as pressuring and ridging. Since these processes are not considered in our model, the comparison for these cases is not as good. We would like to stress that the ice model is not totally mass conserving. However, the ice results show that our simplified approach (no rheology, free drift, and land-fast ice) offers, at least for ice export regions like the Eurasian Arctic shelves, a reasonable and less expensive alternative to complex ice models.

3.1.3. Sea surface salinity (SSS). The seasonal evolution of the SSS is depicted in Figure 10. The river runoff starts in May and June when the fresh water flows mainly to the east. However, in July and August, the freshwater signal from the Ob and Yenisei also propagates northwestward into the central Kara Sea (see detailed discussion in section 3.2.3). Together with the ice melting, the river water also causes a considerable freshening of the surface layers in the central Kara Sea.

The increase of SSS in autumn and winter is most pronounced east of Novaya Semlya and in the Baydaratskaya Bay where thermodynamic ice formation provides a strong salt input through brine release. By the end of March, the fresh surface layer has almost vanished except in the river estuaries and along the Siberian coast.

The general spatial structure of the SSS is well reproduced by the model. Simulated regional differences concerning the seasonal increase and decrease of the SSS are largely supported by descriptions of *Pavlov et al.* [1993]. However, comparisons with almost synoptic observations are difficult. The observed summer SSS in the Kara Sea such as that given by *Milligan* [1969] or *Burenkov and Vasil'kov* [1995] is partly different from the simulated summer climatic mean. This holds true, in particular, for regions north of the estuaries where the observed SSS is lower and frontal structures are more pronounced than in our simulations. This difference can be attributed first of all to the fact that the model uses climatological forcing, whereas the data from *Burenkov and Vasil'kov* [1995], for example, were taken in a year with rather anomalous winds. A second reason might be an insufficient space resolution of the river plume which prejudices the reproduction of frontal structures.

The salt budget for Kara Sea surface waters depends mainly on the ice formation and the river runoff. Previous studies have shown [*Harms*, 1997c] that the yearly averaged, simulated thermodynamic ice production is largely dominated by high net freezing rates along the Siberian coast, with maximum values of

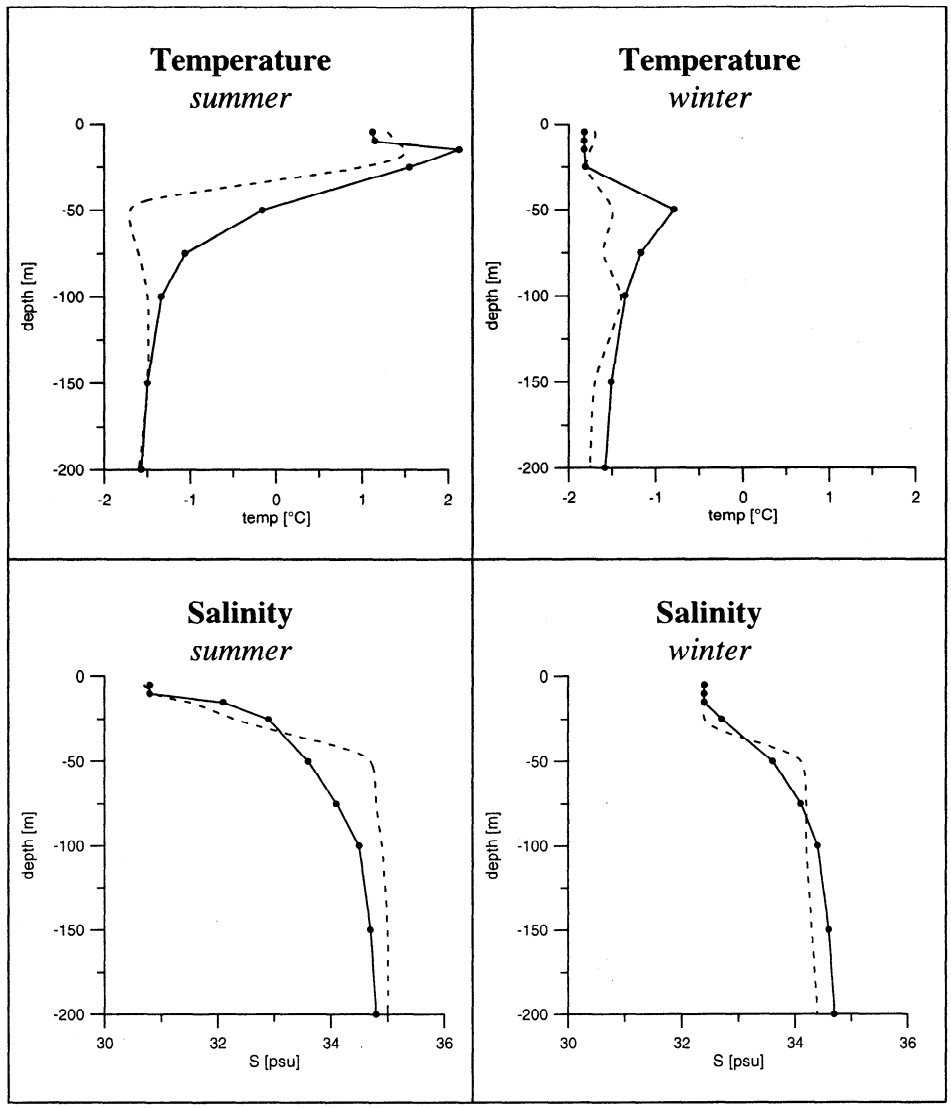

Figure 11. Simulated vertical profiles for temperature and salinity (solid curves) during summer and winter in the Novaya Semlya Trough region. Observations [*Pavlov and Pfirman,* 1995] are shown as dashed curves.

the order of 4 - 6 m/yr. Because of a significant ice export of roughly 150 km^3/yr [*Pavlov et al.,* 1993], the salt input through thermodynamic ice growth in winter is much larger than the corresponding freshwater release through ice melting in spring and summer. This considerable imbalance is largely compensated by the freshwater runoff from the rivers. In this respect, the model underlines the important roles that river runoff, thermodynamic ice growth, and resulting ice export have for the hydrography of the Kara Sea.

However, all these factors are subject to interannual variability. The question to what extent the salt input through ice formation is balanced by the river runoff or by fluxes through open boundaries cannot be answered using climatological forcing fields. Future model studies on the freshwater balance of the Kara Sea should use realistic forcing fields in order to include interannual variations in river runoff and atmospheric forcing.

3.1.4. Stratification. Simulated temperature and salinity profiles for summer and winter are compared to observations in the Novaya Semlya Trough [*Pavlov and Pfirman,* 1995] (Figure 11). Whereas in winter the stratification is generally weak, the summer situation (September) is characterized by a thermohaline stratification, caused by freshwater runoff, ice melting and atmospheric warming. It can be seen from Figure 11 that the model reveals a slight deficiency in maintaining strong vertical gradients from spring until September. However, this is typical for three-dimensional level models with rather simple turbulence closure schemes. More detailed studies on the Kara Sea stratification should probably involve a submodel with a more sophisticated turbulence closure, as suggested for example by *Burchard and Baumert* [1995].

A very strong haline stratification can be observed in late summer/autumn at the Siberian shore when the freshwater plume is established. Vertical density gradients in this area (Figure 12a) are most pronounced in the upper 50 m causing rather strong baroclinic pressure gradients (see also section 3.2.4.). Other typical features of the observed Kara Sea stratification are temperature maxima in 50-100 m depth in autumn, caused by vertical mixing and convection due to atmospheric cooling and ice formation. The model produces a

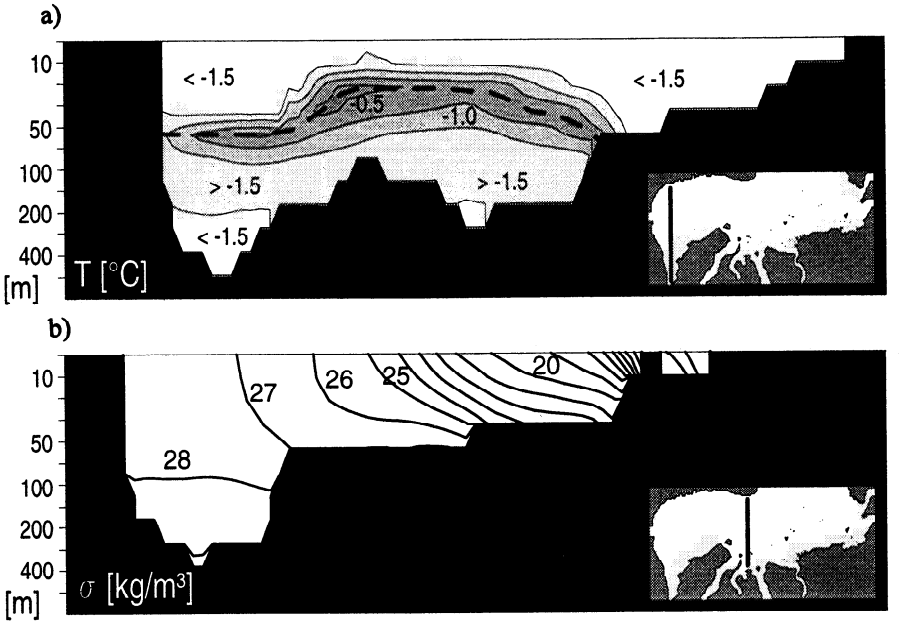

Figure 12. Vertical sections (see inset) through the Kara Sea in autumn, showing (a) vertical density gradients at the Siberian shore and (b) simulated temperature maxima in the central parts of the Kara Sea.

quite pronounced temperature maximum at 50 m depth (Figure 12b) which can be found in the deeper regions of the central Kara Sea. The depth of the temperature maximum depends on the haline stratification which is weaker near the shores of Novaya Semlya and also in the Baydaratskaya Bay. This can be explained by the more saline Barents Sea inflow (see section 3.2.) and intense thermodynamic ice formation along the shore lines [*Pavlov et al.*, 1993].

3.2. Circulation

An overview of the circulation is given by averaged yearly mean fields in section 3.2.1. This gives an impression of the prevailing current systems. The seasonal variance is depicted by surface means of the winter (JFM), spring (AMJ), summer (JAS) and autumn (OND) circulation in section 3.2.2. Special emphasis is given to the surface circulation in regions of freshwater influence (section 3.2.3) and to the sub-surface and near bottom flows (section 3.2.4).

3.2.1. Yearly mean circulation. The model circulation of the upper layers is partly in disagreement with "classical" pictures of the southern Kara Sea circulation. According to *Pavlov et al.* [1993] and *Pavlov and Pfirman* [1995], the general surface circulation should be dominated by a southward going coastal current at the east coast of Novaya Semlya (i.e., the "East Novaya Semlya Current") and a northward going current at the west coast of the Yamal peninsula (i.e., the "Yamal Current"). These two flows should result in a cyclonic circulation pattern in the southern Kara Sea. Unfortunately, no information is given on the seasonal variability of the circulation.

Simulated, yearly averaged flow fields of the upper five layers (0-50 m) do not show this cyclonic circulation (Figure 13). A southward flow along the east coast of Novaya Semlya is completely absent, and the northward flowing Yamal Current is a seasonal feature that appears only in autumn (see section 3.2.2). Instead, the simulated flow field is dominated by topographically guided, northeastward currents that extend from the Kara Strait to Severnaya Semlya and Vilkitsky Strait. Northeastward currents prevail throughout the year along the southeast coast of Novaya Semlya.

The yearly mean surface circulation along the Siberian coast to the east of the Yenisei is dominated by a strong, northeastward flowing coastal current. The flow originates in the river estuaries and leaves through Vilkitsky Strait and west of Severnaya Semlya. In spite of northerly currents at the surface, the near-bottom flow (25-50 m) reveals an undercurrent, flowing at southward directions toward the estuaries.

3.2.2. Seasonal variability of the surface circulation. The simulated sea surface elevation (SSE) in the Kara Sea (Figure 14) is characterized throughout the year by higher levels along the Siberian coast and lower levels along the east coast of Novaya Semlya. This underlines the general northeastward flow which dominates throughout the year in the Kara Sea. However, the SSE gradient varies seasonally, being most pronounced in autumn and winter and weakest in spring and summer. The enhancement in autumn and winter is caused by cyclonic wind fields and the river plume that moves along the Siberian shore. The opposite situation occurs in spring and autumn, when weaker northerly winds prevail and the amount of fresh river water is much smaller.

Despite this dominating SSE gradient, which suggests a more or less prevailing northeastward flow in the Kara Sea, the model reveals a considerable seasonal variability of the surface circulation (Figure 15). The main features can be summarised as follows.

3.2.2.1. Autumn and winter: Current speeds are strongest in autumn during October, November, and December. The general surface flow is from southwest to northeast, caused by strong cyclonic wind fields, pronounced horizontal density and SSE gradients and a maximum inflow from the Barents Sea through the Kara Strait. Because of these factors, the Siberian Coastal Current as well as the Yamal Current are enhanced. At the northern open boundary, outflow from the Kara Sea toward

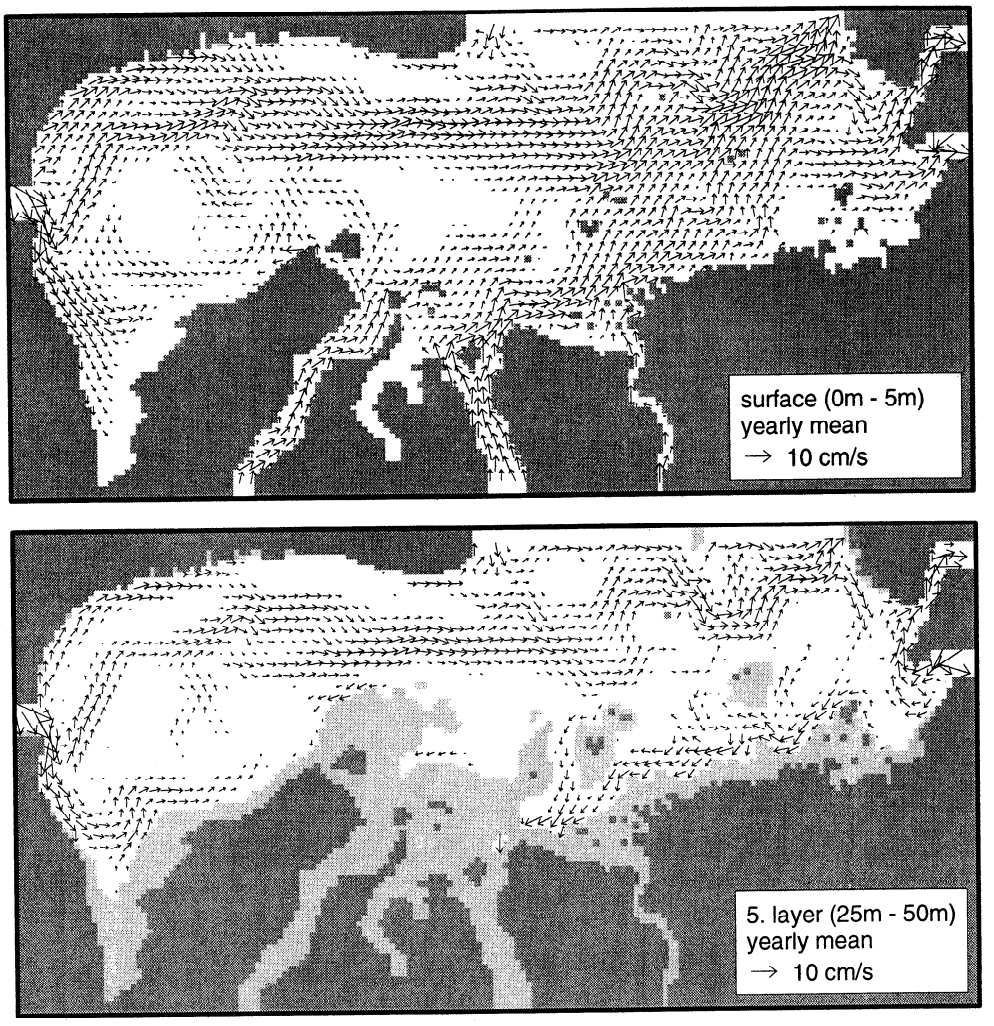

Figure 13. Simulated yearly averaged currents at the surface and in the fifth layer.

the Arctic Ocean dominates. The flow at the southeast coast of Novaya Semlya is to the north.

These circulation patterns are visible also in September, although this month actually belongs to the summer. However, concerning the wind forcing, the September situation is ambiguous. The applied ECMWF climatology, for example, shows a cyclonic autumn wind field already for September. This might explain why observations which were actually made in late summer (September 1994) show good agreement with the simulated autumn circulation. The broad northeastward flow in

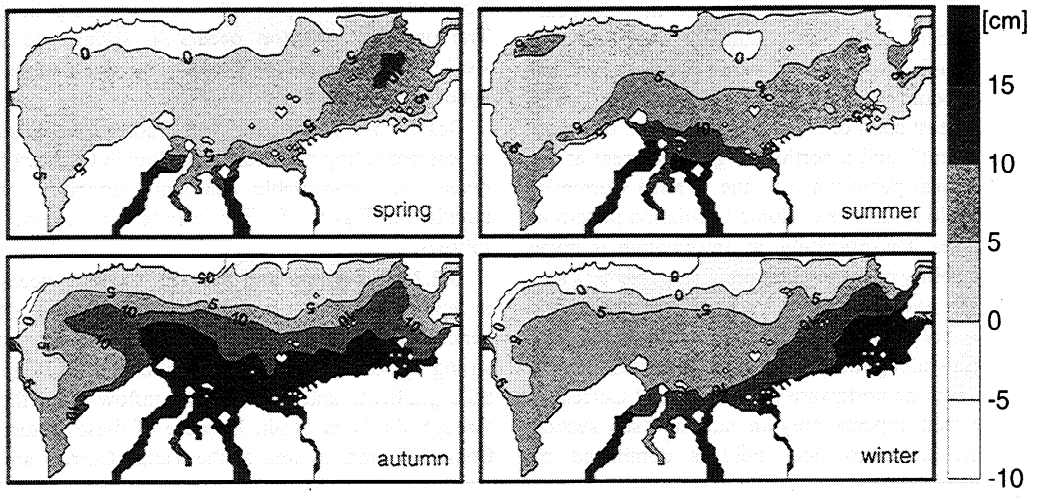

Figure 14. Simulated seasonal mean surface elevations for spring, summer, autumn, and winter.

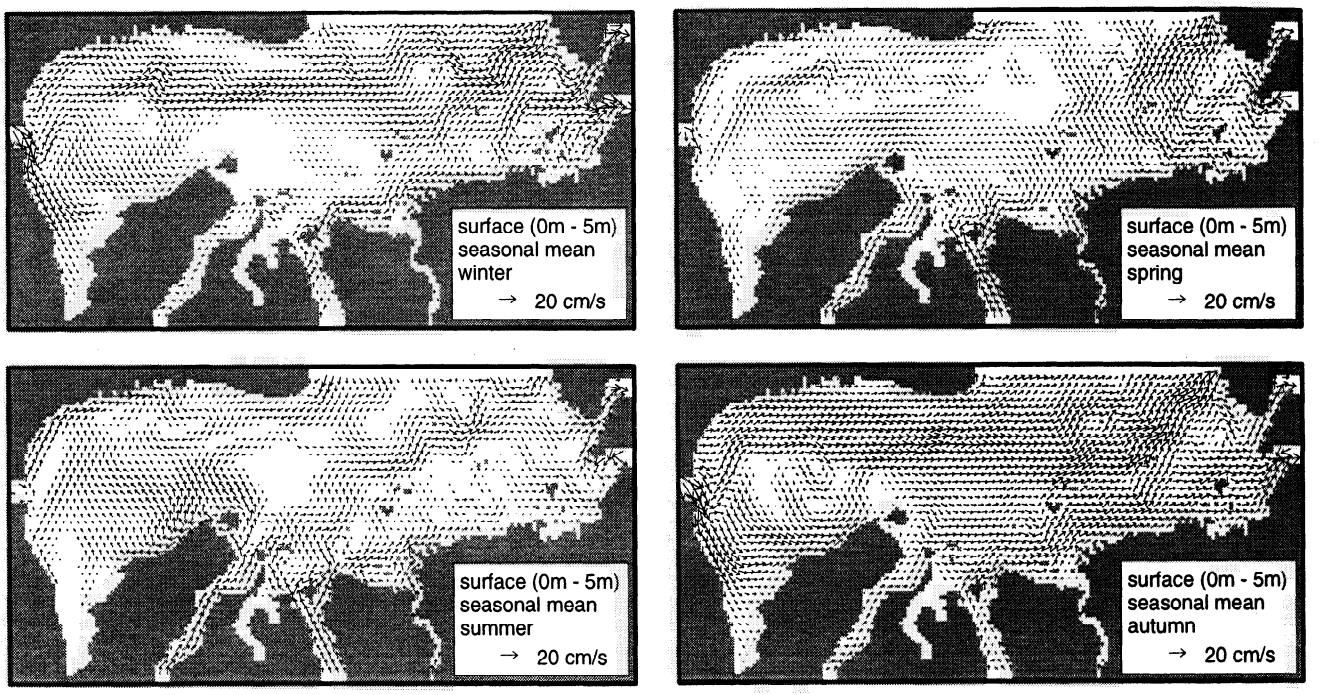

Figure 15. Simulated seasonal mean surface currents for winter, spring, summer, and autumn.

the southern Kara Sea was also found in acoustic Doppler current profiler (ADCP) data [*Johnson et al.*, 1997].

The winter situation in January, February, and March is very similar to autumn, however, current speeds are somewhat weaker in midwinter. This is mostly due to the breakdown of the river runoff and the retreat of the river plume which results in decreasing horizontal density and SSE gradients. A secondary effect is the reduced transfer of momentum from the atmosphere to the ocean because less mobile ice (landfast ice) covers the shallow parts of the sea.

3.2.2.2. Spring and summer: The spring (April, May, and June) and summer (July, August, and September) situation is very different from autumn and winter. It is characterized by weak anticyclonic wind fields and strong river runoff but very weak horizontal density and SSE gradients. The prevailing wind direction is from north to northeast. The Barents Sea inflow through the Kara Strait is small, with slightly negative values in July and August. However, a significant inflow from the Arctic or the Barents Sea around the northern tip of Novaya Semlya can be observed. There is also some inflow from the Laptev Sea through Vilkitsky Strait. This inflow occurs only during spring and summer, when winds are favorable. Westerly currents in Vilkitsky Strait were also observed in 24-hour current meter mooring data recorded during the *Northwind* expedition [*Milligan,* 1969; *Johnson et al.,* 1997]. The general surface circulation pattern in spring tends to be anticyclonic, at least in the southwestern Kara Sea. Apart from enhanced velocities close to the river estuaries, the current speeds in spring and summer are generally much weaker than in autumn.

3.2.3. Region of freshwater influence (ROFI). Although the whole Kara Sea has to be regarded as a ROFI, the freshwater influence is strongest in the estuaries. The seasonal variance of the currents in the Ob and Yenisei estuaries is very pronounced (Figure 16). The currents are strongest during spring and summer when the runoff is large. In spring (May and June), when most parts of the Kara Sea are still covered by ice, the estuarine currents turn sharply to the east. The landfast ice inhibits momentum transfer from the atmosphere, and the flow is mostly density driven. As a result, topographically guided meanders form during May or June, and the horizontal current (and density) shear is considerable. The further retreat of the ice cover in July and August allows the wind to act on the sea surface and to drive the fresh water from the estuaries to the north and northwest. This is reflected in northward currents in the estuaries during July and August. However, the flow at the northern Yamal coast is to the south.

Simulated SSS and also SSE confirm that the summer freshwater signal from the Ob and Yenisei propagates into the central Kara Sea, instead of going mainly eastward as one would expect. A northwestern flow close to the river estuaries was also observed in laboratory simulations by *McClimans* [1997]. Since these simulations were run without any wind forcing, *McClimans* attributed the northward flow of river plumes to tidal rectification. However, in our numerical simulations, the main driving force for the northwestward spreading is the wind. A wind-induced dispersion of river water to the northwest has also been suggested by *Nansen* [1902]. It was later confirmed by *Milligan* [1969] and was recently found by *Johnson et al.* [1997].

From September on, when the freshwater plume has its largest extent, the winds change to the cyclonic winter situation. Large amounts of freshwater are pushed back to the Siberian shore, and a pronounced coastal current develops that prevails throughout the autumn and early winter. At the same time, "high" saline water from the southwestern Kara Sea flushes the west coast of the Yamal peninsula. It penetrates into the freshwater plume north of Yamal and cuts it off from the coast (see Figure 10, X, XI, XII). As a result, isolated lenses of low-saline river water remain in the southern Kara Sea. Very similar observations were made by *Burenkov and Vasil'kov* [1995], who

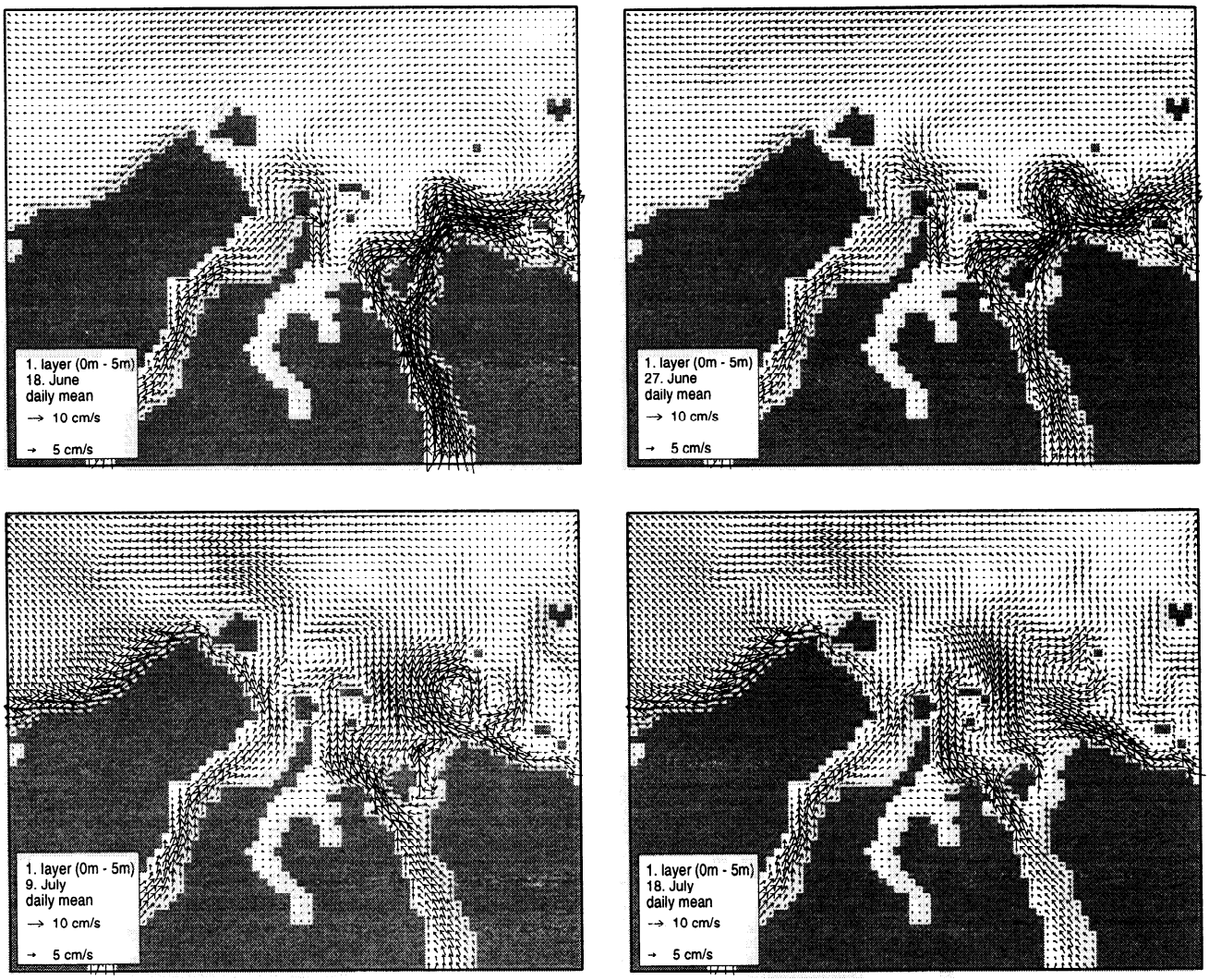

Figure 16. Simulated daily mean surface currents for four selected days from June 18 to July 18.

found exceptionally low-salinity values in freshwater lenses east of Novaya Semlya. The high silicate content of this water showed that the observed lens was related to river discharge. *Burenkov and Vasil'kov* suggest that these lenses are formed through detachment of the Ob and Yenisei river plume from the coast.

In preliminary dispersion studies [*Karcher et al.*, 1997], tracers were released in the Ob and Yenisei estuaries during peak runoff. These simulations showed that the spreading and the transit times depend very much on the tracer depth (see also section 3.2.4). Whereas surface river tracers usually need less than 2 years to leave the model domain, near-bottom tracers might circulate for several years in the central Kara Sea. This holds in particular for "deep" Ob tracers that spread to a large extent in the southwestern Kara Sea.

3.2.4. Sub-surface and near bottom flows. The seasonal variance in the deeper layers is much weaker than at the surface. Examples are given for the fifth model layer, between 25 and 50 m (Figure 17), which usually coincides with the lower boundary of the upper thermo-haline stratification (see section 3.1.4). The seasonal variance in these depths is confined to two circulation types for either spring/summer or autumn/winter. However, the differences between summer and autumn circulation concerns mainly the flow intensities. Because of a permanent SSE gradient (c.f. Figure 14), a northeastward flow dominates in both seasons the circulation along the southeast coast of Novaya Semlya and in the central Kara Sea.

In both seasons, summer and autumn, a southwestward undercurrent flows at 5-10 cm/s along the Siberian shores in the opposite direction to the surface flow. In our model simulations, the main driving force for this flow is a strong baroclinic pressure gradient (see also section 3.1.4. and Figure 12a) that opposes the barotropic one, stemming from the SSE field. The most favorable season for this case is late summer, when the river plume is fully established and the wind and SSE fields still reflect the summer situation. The Siberian undercurrent is therefore strongest in late summer and weakest or absent in late winter or spring. Recent observations and modeling efforts support our findings: vertical current shear was also found at current meter moorings deployed close to the Ob and Yenisei estuaries in autumn [*Johnson et al.*, 1997] and also in laboratory model studies by *McClimans* [1997]. However, in both cases the observed underflow was slightly weaker as in our simulations.

The strongest seasonal variability in depths between 25 and 50 m can be found at the Yamal coast. Northward currents prevail only during autumn and winter, whereas in spring and

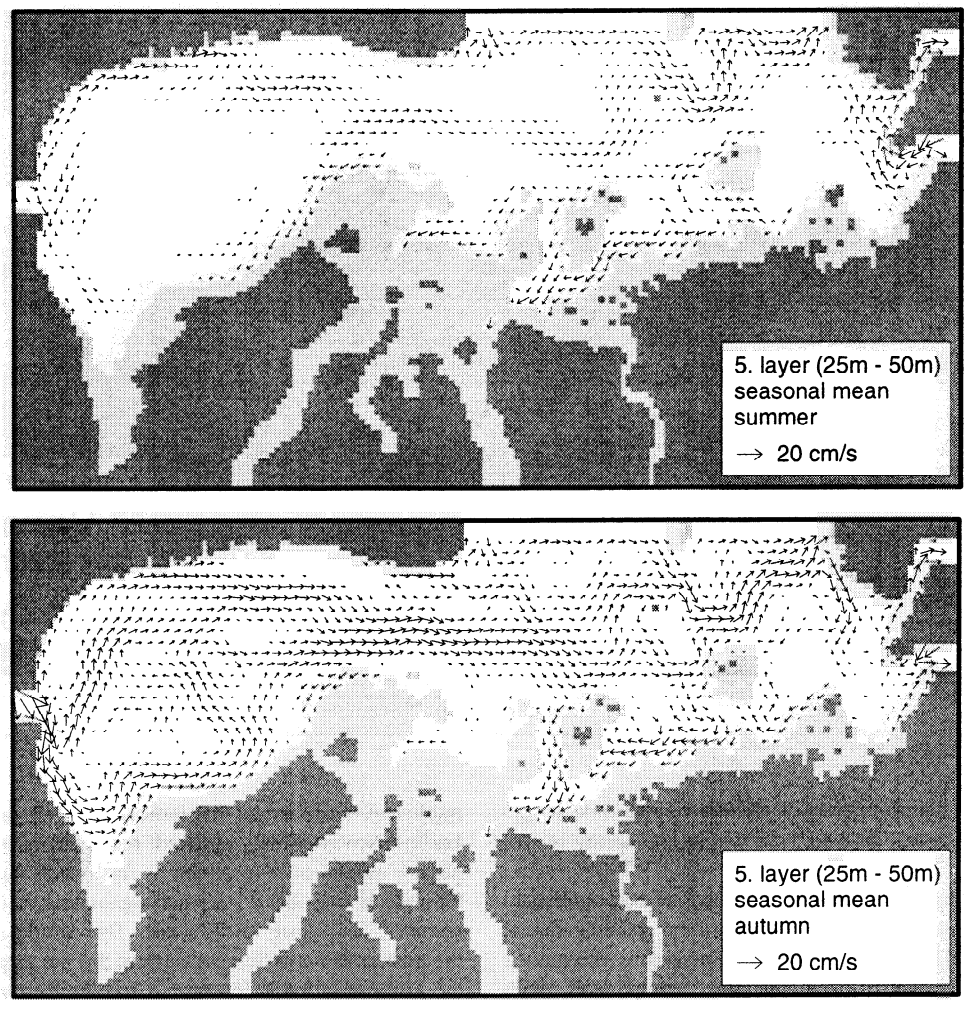

Figure 17. Simulated seasonal mean currents for summer and autumn in the fifth layer.

summer the flow is southward. This is very similar to the surface circulation, suggesting a barotropic current profile. The wind fields and the related SSE are the main driving forces for this flow.

The deep flows in the seventh layer, between 75 and 100 m (Figure 18), are mainly driven by barotropic pressure gradients originating from the Kara Strait inflow and the wind fields. A strong topographic steering can be observed, which results in two recirculation cells just to the east of the Kara Strait. The inflow from the Barents Sea first moves in a southern loop into Baydaratskaya Bay before returning to the Kara Strait again. There the broad northward flow partly recirculates in a northern loop that also returns to the Kara Strait, this time by flowing southward along the coast of Novaya Semlya. Very similar recirculation cells were reported from laboratory tracer experiments by *McClimans* [1997]. These recirculation patterns suggest that (1) the inflowing water masses from the Barents Sea may return with a westward flow to the Kara Strait and (2) the residence times for inflowing Barents Sea water masses or contaminants in the southern Kara Sea may be prolonged.

After passing the recirculation cells to the east of the Kara Strait, the northeastward flow continues through the central Kara Sea toward Severnaya Semlya and the Vilkitsky Strait. The seasonal variance in these depths is small and mostly confined to the flow intensity. The described flow field with maximum current speeds of more than 10 cm/s close to the Kara Strait dominates from November to March. In summer, the flow is significantly weaker, but there is no reverse in the current direction.

4. Summary and Final Remarks

Summarizing the main results of the present model study, it can be said that the yearly averaged flow field is dominated by the autumn situation, because this season shows the strongest circulation. However, there is no typical "Kara Sea circulation" that prevails throughout the year. The model results revealed a pronounced seasonal variability that is caused by the wind field, the freshwater runoff, and the ice formation. This variability concerns not only the circulation but also the hydrography.

An evaluation of the Kara Sea model is difficult, first of all because direct observations are scarce or unpublished and second because the application of climatological forcing fields in prognostic model simulations leads to "artificial" results that do not reflect a real or observed situation. This allows only for a qualitative comparison between climatological model results and direct measurements. Another problem arises from the fact that most of the available observations were made during summer.

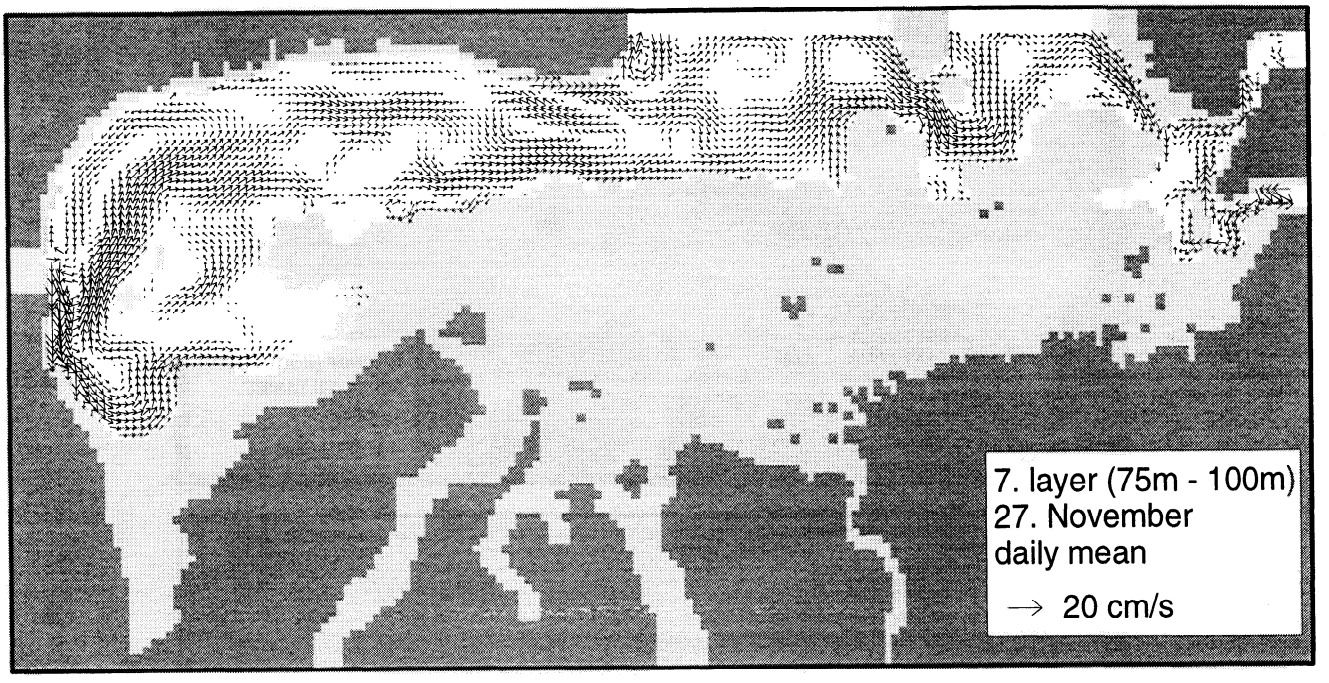

Figure 18. Simulated daily mean currents for November 27 in the seventh layer.

There is almost no information on the remaining time of the year, which makes a validation of our winter and spring results difficult.

The simulated hydrography is found to be in good agreement with available observations. In particular, the general spatial structure of the SST and SSS is well reproduced by the model. Some differences were found in the comparison with measurements; the observed summer SSS in the Kara Sea ROFI is somewhat lower than in the simulations. This can be attributed to the climatic forcing but also to an insufficient horizontal resolution by the model. Similar problems occurred in the vertical, where the model showed some deficiencies in maintaining the strong summer stratification for 2 or 3 months. Future model studies should consider these points by using a higher spatial resolution, sophisticated turbulence closure schemes, and realistic forcing fields on the basis of, for example daily means.

Concerning the simulated circulation, we found a very good agreement between our model results and the available observations in several areas. Laboratory modeling results seem to support the numerical model results on several points. Some discrepancies appeared when we compare the model simulations with the oceanographic descriptions of the Kara Sea given by *Pavlov et al.* [1993] and *Pavlov and Pfirman* [1995]. The described hydrography agrees well with our model results, but there were some differences concerning the circulation. The frequently cited cyclonic current pattern which should dominate the circulation in the central and southern Kara Sea is not (or only partly) present in our model simulations. The main reasons for this are (1) the absence of the Eastern Novaya Semlya Current and (2) the strong seasonality of the Yamal Current that appears only in autumn in our simulations.

As mentioned previously, the simulated flow along the east coast of Novaya Semlya is generally weak and mostly to the north. This agrees with a drifter trajectory [*Føyn and Nikitin*, 1994] from August to September 1994. Although this is a very weak and maybe also an incidental support, we found no published observations that indicated a flow to the south. If the Eastern Novaya Semlya Current really exists, it might be a very narrow coastal current, driven by freshwater runoff from Novaya Semlya. It may be a seasonal signal that is only observed in summer, very close to the coast. This would also explain why the Eastern Novaya Semlya Current did not appear in the model: the grid resolution is too coarse and the freshwater runoff from Novaya Semlya is not included.

The discrepancy concerning the simulated and observed Yamal Current can probably be explained in the same way. The northward flowing Yamal current was mainly observed in autumn when climate and weather are favorable. This leads to the "traditional" but probably wrong impression that northward currents prevail throughout the year at the Yamal coast.

These are only two attempts to explain the differences between the model results and the traditional picture of the Kara Sea circulation. The authors do not claim that the model is right and the traditional view is wrong. However, without detailed observations, it cannot be definitely concluded whether the Kara Sea circulation really behaves according to the traditional view or not.

Two more simulated features seem to be important not only for the Kara Sea circulation but also for contaminant transport: the southward, near-bottom flow below the Siberian Coastal Current and two recirculation cells that appear in the deeper layers east of the Kara Strait. For both features, we found some agreement with recent observations and laboratory modeling. However, the present model results underline the urgent need for more information on the Kara Sea circulation and hydrography.

5. Outlook

The achieved circulation results will be used for tracer dispersion simulations in order to study the major pathways for contaminants in the Kara Sea [*Nies et al.*, 1997; *Karcher et al.*, 1997]. This also concerns terrigenous substances in ice and

water, its accumulation on the shelf, and its transport from the shelf into the open ocean environment. The sediment supply to the Kara Sea and the deep Arctic basins is mainly controlled by river discharges. From more than 30 million tons of suspended material that is discharged annually into the Kara Sea, only 0.47 million tons (1.5%) are believed to leave the shelf. In contrast, 80% of the dissolved matter discharged by rivers is expected to enter the Arctic Ocean [*Schlosser et al.*, 1995]. As the model results have shown previously, the inflowing fresh water causes a strong seasonality in hydrography and circulation on the shelf. The same strong seasonality can be assumed for the input of dissolved and particulate matter from the rivers. The peak release of suspended matter by the rivers might be even more pronounced than the freshwater signal itself. With respect to sediment transport in water and sea ice, it is interesting to mention that simulated ice velocities, surface currents, and near-bottom flows in the river estuaries might have considerable differences in direction. However, this is a subject for ongoing investigations and will be discussed in a future publication.

Acknowledgments. This work was funded by the German Ministry for Education, Research, Science and Technology (BMBF, 02-E-87054). Some of the topographic and M_2 tidal data were kindly provided by Igor Polyakov and Andrey Proshutinsky, University of Fairbanks, Alaska. Information on the Arctic river runoff was compiled and provided by O.F. Vasiliev, G.A. Orlova, and E.A. Korobkina from the Institute for Water and Environmental Problems, Siberian Branch, Russian Academy of Sciences, Novosibirsk. We are grateful to Hartmut Nies and Jan Backhaus for help and support. Thanks also to Igor Polyakov, Tom McClimans, and one anonymous reviewer for constructive comments and criticism. Jennifer Verduin checked the manuscript; many thanks go to her.

References

Aukrust, T., and J.M. Oberhuber, Modelling of the Greenland, Iceland and Norwegian Seas with a coupled sea ice - mixed layer - isopycnal ocean model, *J. Geophys. Res., 100 (C3)*, 4771-4789, 1995.

Backhaus, J.O., A three-dimensional model for the simulation of shelf sea dynamics, *Dsch. Hydrogr. Z.*, 38 (H4), 165-187, 1985.

Bruno, M.S., and O.S. Madsen, Coupled circulation and ice floe movement model for partially ice-covered continental shelves, *J. Geophys. Res., 94 (C2)*, 2065-2077, 1989.

Burchard, H., and H. Baumert, On the performance of a mixed-layer model based on the k-e turbulence closure, *J. Geophys. Res., 100 (C5)*, 8523-8540, 1995.

Burenkov, V.I., and A.P. Vasil'kov, The influence of runoff from land on the distribution of hydrologic characteristics of the Kara Sea, *Oceanology of the Antarctic Shelf, Antarct. Res. Ser.*, vol. 34, no. 5, pp. 591-599, AGU, Washington D.C., 1995.

Cherkis, N.Z., H.S. Fleming, M.D. Max, and M.F. Czarnecki, Bathymetry of the Barents and Kara Seas, *Sea Chart*, Nav. Res. Lab., Washington, D. C., 1990.

European Centre for Medium Range Weather Forecasts (ECMWF), ECMWF Forecast Model, Physical parameterization, *Res. Manual 3*, 2nd ed., Reading, England, 1988

Føyn, L., and A. Nikitin, The joint Norwegian-Russian expedition to the dump sites for radioactive waste in the Abrasimov Fjord and the Stepovogo Fjord, August-September 1994, cruise report, Inst. of Mar. Res., Bergen, Norway, 1994.

Gjevik, B., and T. Straume, Model simulations of the M2 and the K1 tides in the Nordic Seas and the Arctic Ocean, *Tellus,Ser. A,41*, 73-96, 1989.

Gloersen, P., W.J. Campbell, D.J. Cavalieri, J.C. Comiso, C.L. Parkinson and H.J. Zwally, Arctic and Antarctic Sea Ice, 1978-1987: Satellite passive-microwave observations and analyses, *NASA Spec. Publ., SP-511*, 290 p., 1992.

Gorshkov, S.G., *Atlas of Oceans*, Arctic Ocean Mil. Def. Publ., Moscow, 1980.

Harms, I.H., Numerische Modellstudie zur winterlichen Wassermassenformation in der Barentssee, Berichte aus dem Zentrum für Meeres- und Klimaforschung der Universität Hamburg, Reihe B: Ozeanographie, Nr. 7, 97 p., 1994.

Harms, I.H., Water mass transformation in the Barents Sea, *J. Mar. Sci., 54*, 1997a.

Harms, I.H., Modelling the dispersion of ^{137}Cs and ^{239}Pu released from dumped waste in the Kara Sea, *J. Mar. Syst., 13*, 1-19, 1997b.

Harms, I.H., Freshwater runoff and ice formation in Arctic Shelf Seas: Results from a high resolution Kara Sea model, *in Proceedings of the "WCRP/ACSYS Conference on Polar Processes and Global Climate"*, draft summary report, Arct. Clim. Syst. Study Proj. Off., Oslo, 1997c.

Hibler, W.D., III, A dynamic thermodynamic sea ice model, *J. Phys. Oceanogr., 9*, 815-846, 1979.

Hirtzler, J.D. (ed.), Relief of the surface of the Earth, *in MGG-2, Natl. Geogr. Data Cent.*, Boulder, Colo., 1985.

Johnson, D.R., T.A. McClimans, S. King and Ø. Grenness, Fresh water masses in the Kara Sea during summer, *J. Mar. Syst., 12*, 127-145, 1997.

Joint Russian-Norwegian Expert Group, Dumping of radioactive waste and investigation of radioactive contamination in the Kara Sea. Results from 3 years of investigations (1992-1994) in the Kara Seas, report, Norw. Radiat. Prot. Auth., Osteras, Norway, 1996.

Karcher, M.J., and J.M. Oberhuber, Modeling the ventilation of the upper and intermediate water of the Arctic Ocean with an isopycnic model, in *"WCRP/ACSYS Conference on Polar Processes and Global Climate"*, draft summary report, Arct. Clim. Syst. Study Proj. Off., Oslo, 1997.

Karcher, M.J., I.H. Harms, D. Dethleff and H. Nies, Transit times and pathways of contaminants in the Arctic Ocean, paper presented at "The AMAP International Symposium on Environmental Pollution of the Arctic", June 1-5, 1997, Tromsø, Norway, 1997.

Kochergin, V.P., Three-dimensional prognostic models, in *Three-Dimensional Coastal Ocean Models,Coastal Estuarine Stud.*, vol. 4, edited by N. Heaps, pp. 201-208, AGU, Washington, D. C., 1987.

Kowalik, Z., and A.Y. Proshutinsky, Diurnal tides in the Arctic Ocean, *J. Geophys. Res., 98 (C9)*, 16449-16468, 1993.

Kowalik, Z., and A.Y. Proshutinsky, The Arctic Ocean tides, in *The Polar Oceans and Their Role in Shaping the Global Environment*, edited by O.M. Johannessen, R.D. Muench, and J.E. Overland, pp. 131-158, *Geophys. Monogr. Ser., vol. 85*, AGU, Washington, D. C., 1994.

Lemke, P.,W.B. Owens, and W.D. Hibler, A coupled sea ice mixed layer pycnocline model for the Wedell Sea, *J. Geophys. Res., 95 (C6)*, 9513-9525, 1990.

Levitus, S., Climatological atlas of the world ocean, *NOAA Prof. Pap., 13*, 1982.

Maykut, G.A., The surface heat and mass balance, in *Geophysics of Sea Ice*, edited by N. Untersteiner, NATO ASI Ser., 146, pp. 395-463, 1986.

McClimans, T.A., Model verification of transport processes in the Barents and Kara Seas, paper presented at "The AMAP International Symposium on Environmental Pollution of the Arctic", June 1-5, 1997, Tromsø, Norway, 1997.

McPhee, M.G., The effect of the oceanic boundary layer on the mean drift of pack ice: Application of a simple model, *J. Phys. Oceanogr., 9*, 388-400, 1979.

Mellor, G.L., and T. Yamada, A hierachy of turbulence closure models for planetary boundary layers, *J. Atmos. Sci., 31*, 1791-1806, 1974.

Milligan, D., Oceanographic survey results: Kara Sea, summer and fall 1965, *Techn. Report, TR-217*, U.S. Nav. Oceanogr. Off., Washington D. C., 1969.

Moe, K.A., R. Hansson, and J. Thomassen, Strategic environmental impact assessment: The Northern Sea Route (Russia). Results obtained during phase I of the International Northern Sea Route Programme (INSROP), paper presented at *"The AMAP International Symposium on: 'Environmental Pollution in the Arctic"*, June 1-5 1997, Tromsø, Norway.

Nansen, F., Oceanography of the North Polar Basin, in *The Norwegian North Polar Expedition 1893-1896*, edited by F. Nansen, *Sci. Res., V (IX)*, 427 p., 1902.

Nies, H., C. Bahe, D. Dethleff, I. Harms, M. Karcher, and E. Kleine, Transport and dispersion of artificial radioactivity in the Arctic Ocean, *Radioprotection - Colloques, 32 (C2)*, 407-416, 1997.

Nilsson, A., Arctic pollution issues: A state of the Arctic environment report, *Arct. Monit. and Assess. Progr., AMAP*, Oslo, Norway, 1997.

Pavlov, V.K. and S.L. Pfirman, Hydrographic structure and variability

of the Kara Sea: Implications for pollutant distribution, *Deep Sea Res. II, part 42 (6)*, pp.1369-1390, 1995.

Pavlov, V.K., M.Y. Kulakov, and V. Stanovoy, Oceanographical Description of the Kara and Barents Sea, report, Int. At. Energy Agency, Vienna, Austria, 1993.

Perry, R.K., and H.S. Fleming, Bathymetry of the Arctic Ocean, *Sea Chart*, Nav. Res. Lab., Washington, D. C., 1986.

Pfirman, S.L., J.W. Kögeler, and I. Rigor, Potential for rapid transport of contaminants from the Kara Sea, *Sci. of the Total Environ., 202*, pp.111-122, 1997.

Pohlmann, T., Calculating the annual cycle of the vertical eddy viscosity in the North Sea with a three-dimensional baroclinic shelf sea circulation model, *Cont. Shelf Res., 16 (2)*, 147-161, 1996.

Romanov, I.P., *Atlas of Ice and Snow of the Arctic Basin and Siberian Shelf Seas*, 2nd ed., edited by A. Tunik, Backbone, New York, 1995.

Schlosser, P., J.H. Swift, D. Lewis, and S. Pfirman, The role of the large-scale Arctic Ocean circulation in the transport of contaminants, *Deep Sea Res. II*, 42 (6), pp. 1341-1367, 1995.

Scott, E.M., P. Gurbutt, I. Harms, R. Heling, S.P. Nielsen, I. Osvath, R. Preller, T. Sazykina, K.L. Sjoeblom and A. Wada, Benchmarking of numerical models describing the dispersion of radionuclides in the Arctic Seas, *Sci. of the Total Environ., 202*, pp.123-134, 1997.

Stronach, J.A., J.O. Backhaus, and T.S. Murty, An update on the numerical simulation of oceanographic processes in the waters between Vancouver Island and the mainland: The GF8 model, *Oceanogr. Mar. Biol., 31*, pp.1-86, 1993.

Trenberth, K.E., J.G. Olson, and W.G. Large, A global ocean wind stress climatology based on ECMWF analyses, *NCAR Tech. Note NCAR/TN-338+STR*, 93 pp., Natl. Cent. for Atmos. Res., Boulder, Colo., 1989.

Yablokov, A.V., V.K. Krasev, V.M. Rumyantsev, M.Y. Kokeyev, O.I. Petrov, V.N. Lystsov, A.F. Yemelyanenkov, and P.M. Rubtsov, *Facts and Problems Related to Radioactive Waste Disposal in Seas Adjacent to the Territory of the Russian Federation*, English transl., Small Word Publ., Alberquerque, N. M., 1993.

I.H. Harms, Institute for Marine Research, University of Hamburg, Troplowitzstrasse 7, D-22529 Hamburg, Germany.
(harms@ifm.uni-hamburg.de)

M.J. Karcher, Alfred-Wegener-Institute for Polar and Marine Research, Columbusstrasse, D-27568 Bremerhaven, Germany.
(mkarcher@awi-bremerhaven .de)

(Received March 11, 1998; revised September 20, 1998;
Accepted February 8, 1999.)